Imaging of Macular Diseases with Optical Coherence Tomography

Carmen A. Puliafito, MD,[1] Michael R. Hee, MS,[2] Charles P. Lin, PhD,[1] Elias Reichel, MD,[1] Joel S. Schuman, MD,[1] Jay S. Duker, MD,[1] Joseph A. Izatt, PhD,[2] Eric A. Swanson, MS,[3] James G. Fujimoto, PhD[2]

Background/Purpose: To assess the potential of a new diagnostic technique called optical coherence tomography for imaging macular disease. Optical coherence tomography is a novel noninvasive, noncontact imaging modality which produces high depth resolution (10 μm) cross-sectional tomographs of ocular tissue. It is analogous to ultrasound, except that optical rather than acoustic reflectivity is measured.

Methods: Optical coherence tomography images of the macula were obtained in 51 eyes of 44 patients with selected macular diseases. Imaging is performed in a manner compatible with slit-lamp indirect biomicroscopy so that high-resolution optical tomography may be accomplished simultaneously with normal ophthalmic examination. The time-of-flight delay of light backscattered from different layers in the retina is determined using low-coherence interferometry. Cross-sectional tomographs of the retina profiling optical reflectivity versus distance into the tissue are obtained in 2.5 seconds and with a longitudinal resolution of 10 μm.

Results: Correlation of fundus examination and fluorescein angiography with optical coherence tomography tomographs was demonstrated in 12 eyes with the following pathologies: full- and partial-thickness macular hole, epiretinal membrane, macular edema, intraretinal exudate, idiopathic central serous chorioretinopathy, and detachments of the pigment epithelium and neurosensory retina.

Conclusion: Optical coherence tomography is potentially a powerful tool for detecting and monitoring a variety of macular diseases, including macular edema, macular holes, and detachments of the neurosensory retina and pigment epithelium.

Ophthalmology 1995;102:217–229

Originally received: May 31, 1994.
Revision accepted: August 23, 1994.

[1] New England Eye Center, Tufts University School of Medicine, Boston.

[2] Department of Electrical Engineering and Computer Science and Research Laboratory of Electronics, Massachusetts Institute of Technology, Cambridge.

[3] Lincoln Laboratory, Massachusetts Institute of Technology, Lexington.

Supported in part by NIH grant RO-1-GM35459-08, Bethesda, Maryland; MFEL grant N00014-91-C-0084, Arlington, Virginia; Air Force grant F49620-93-1-0301; an unrestricted departmental grant from Research to Prevent Blindness, New York, New York; and the Massachusetts Lions Eye Research Fund, Inc, Massachusetts.

Drs. Puliafito and Fujimoto are consultants for Humphrey Instruments, Inc, San Leandro, California.

Reprint requests to Carmen A. Puliafito, MD, New England Eye Center, Tufts University School of Medicine, 750 Washington St, Box 450, Boston, MA 02111.

High-resolution cross-sectional imaging of the retina may be useful for identifying, monitoring, and quantitatively assessing macular diseases. However, current diagnostic instruments lack sufficient resolution to provide useful cross-sectional images of retinal structure. The resolution of standard clinical ultrasound is limited by the wavelength of sound in ocular tissue to approximately 150 μm.[1,2] High-frequency ultrasound biomicroscopy offers a resolution of approximately 20 to 40 μm; however, its penetration into the eye is limited to the first 4 mm of the anterior segment.[3] Ocular aberrations and the maximum entrance pupil diameter of the eye limit the longitudinal resolution of confocal imaging techniques such as scanning laser ophthalmoscopy[4] and scanning laser tomography[5] to approximately 300 μm.

We have developed a new diagnostic technique for high-resolution, noncontact imaging of the human retina

called optical coherence tomography (OCT).[6–12] Optical coherence tomography is analogous to ultrasound, except that optical rather than acoustic reflectivity is measured. Cross-sectional images of optical reflectivity in the retina are obtained similar to ultrasound B-scan, but with a 10-μm longitudinal resolution. Unlike ultrasound, contact between the probe module and the eye is not required so that slit-lamp biomicroscopy of the retina is possible simultaneous with image acquisition. In previous reports, we have demonstrated in vivo OCT imaging of the normal human retina and anterior segment.[11,12] We have shown that OCT tomographs of the posterior pole can distinguish the cross-sectional morphology of the fovea and optic disc, the layered structure of the retina, and normal variations in retinal and retinal nerve fiber layer thickness.[11]

In this article, we describe the first clinical examination of macular diseases using OCT. Optical tomography was performed in patients with selected macular pathologies and correlated with fundus examination and fluorescein angiography. We show that the high-resolution, cross-sectional view of the macula provided by OCT can be a potentially powerful tool for diagnosing and monitoring a variety of macular diseases, including macular edema, macular holes, and detachments of the neurosensory retina and pigment epithelium.

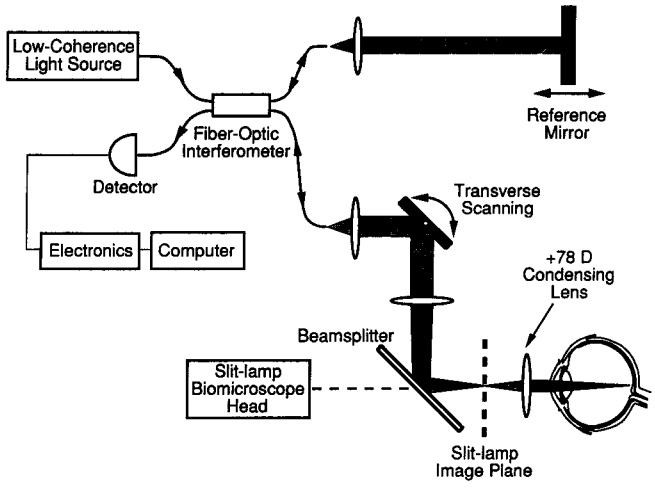

Figure 1. Schematic diagram of the optical coherence tomography system. Axial profiles of backscattering (A-scans) within the eye are measured by translating the reference mirror and recording the interferometric signal. Cross-sectional tomographs of optical reflectivity are constructed analogous to ultrasound B-scan by scanning the probe beam across the fundus.

Materials and Methods

In OCT, the time-of-flight delay of light reflected or backscattered from different depths in tissue is determined with high precision using low-coherence interferometry. We have developed a high-speed fiber optic OCT scanner which is coupled to a standard slit-lamp biomicroscope so that OCT imaging may be performed as an adjunct to conventional retinal examination. A detailed description of this technique may be found in our previous publications.[6–12] Briefly, low-coherence light is coupled into a fiber optic Michelson interferometer (Fig 1). A superluminescent diode light source (a laser diode containing an anti-reflection–coated output facet) is used to provide a bright source of spatially uniform, low-coherence light. One of the two fiber optic arms of the interferometer emits the probe beam and is used for both illumination of the retina and for collection of reflected light. Time-of-flight information is contained in the interference signal between this reflected probe beam and light returning from a reference optical delay path, and is detected by a photodiode followed by signal processing electronics and computer data acquisition. A constant refractive index of 1.36 is assumed to convert time-of-flight delay into a distance within the retina. The depth resolution of OCT imaging depends only on the source coherence length, which essentially describes the maximum optical path length mismatch between the sample and reference interferometer paths that will produce an interference signal at the detector. The source coherence length defines the ideal longitudinal point-spread-function of the OCT imaging system and was experimentally determined to be 14 μm full width at half-maximum in air by measuring the width of the reflection from a mirror placed in the sample arm of the interferometer. This measurement agrees with theoretical calculations based on the spectral characteristics of the source and predicts a longitudinal resolution of 10-μm full width at half-maximum in the retina after accounting for the difference in refractive index between air and tissue. It is important to note that the temporal coherence property of the source, and consequently the longitudinal resolution, is independent of both the optical

Top, Figure 2. Cross-sectional optical coherence tomography image obtained from a normal human macula. Identifiable features include the vitreous, posterior hyaloid, fovea, retinal nerve fiber layer (RNFL), inner and outer plexiform layers (IPL, OPL), photoreceptor layer (PRL), and a highly reflective (red) band corresponding to the retinal pigment epithelium and choriocapillaris.

Second row, Figure 3. Case 1. Idiopathic full-thickness macular hole, right eye. **Second row left,** fundus photograph. **Second row right,** optical coherence tomography image shows a full-thickness defect of the retina, cystoid changes, and a halo of retinal detachment.

Third row, Figure 4. Case 2. Idiopathic full-thickness macular hole with operculum, left eye. **Third row left,** fundus photograph. **Third row right,** optical coherence tomography image shows a full-thickness loss of retinal tissue and an associated operculum.

Bottom, Figure 5. Case 3. Lamellar macular hole, left eye. **Bottom left,** fundus photograph. **Bottom right,** optical coherence tomography image shows a partial depletion of retinal tissue corresponding to the hole.

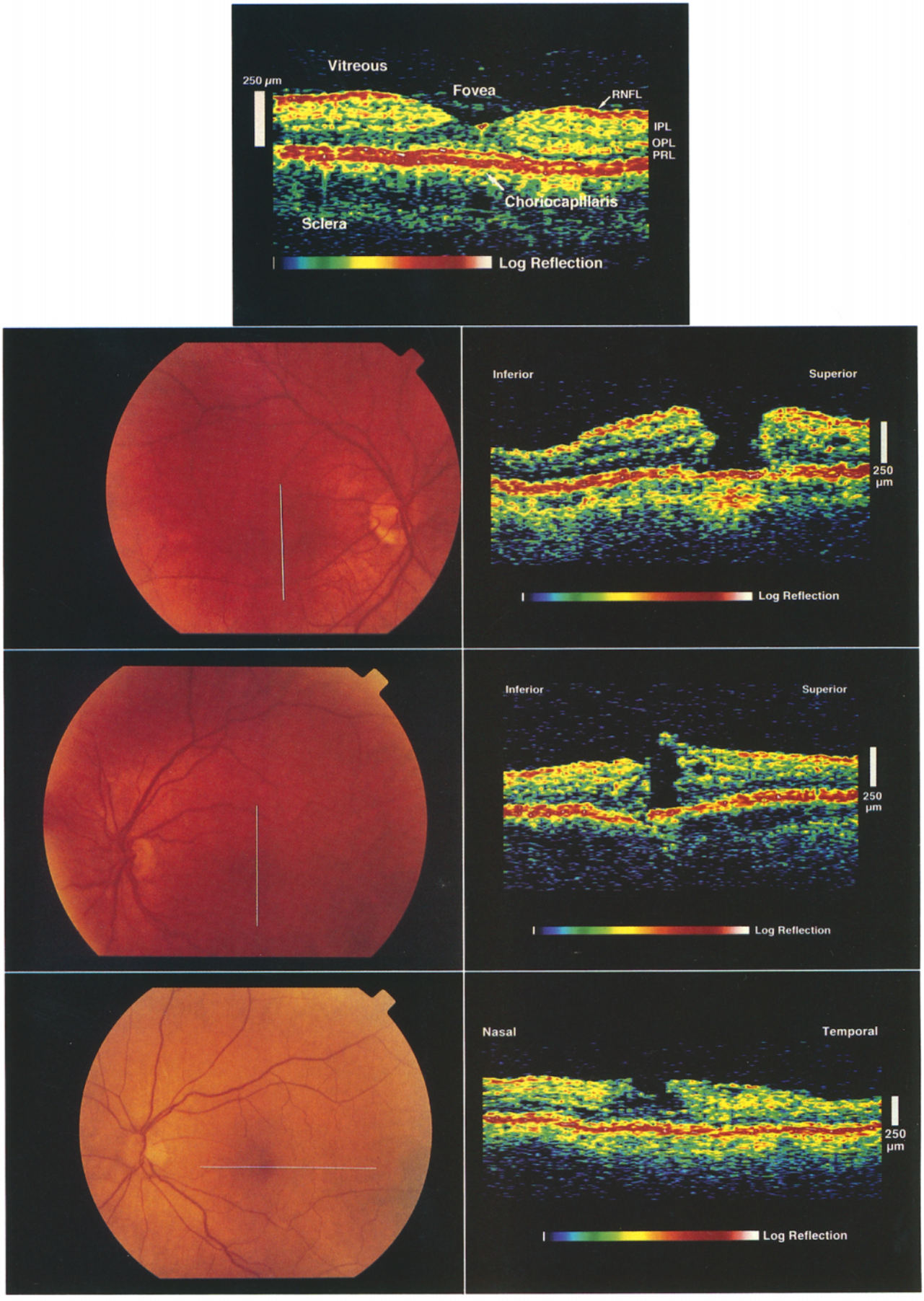
Vitreous
250 μm
Fovea
RNFL
IPL
OPL
PRL
Choriocapillaris
Sclera
Log Reflection
Inferior
Superior
250 μm
Log Reflection
Inferior
Superior
250 μm
Log Reflection
Nasal
Temporal
250 μm
Log Reflection

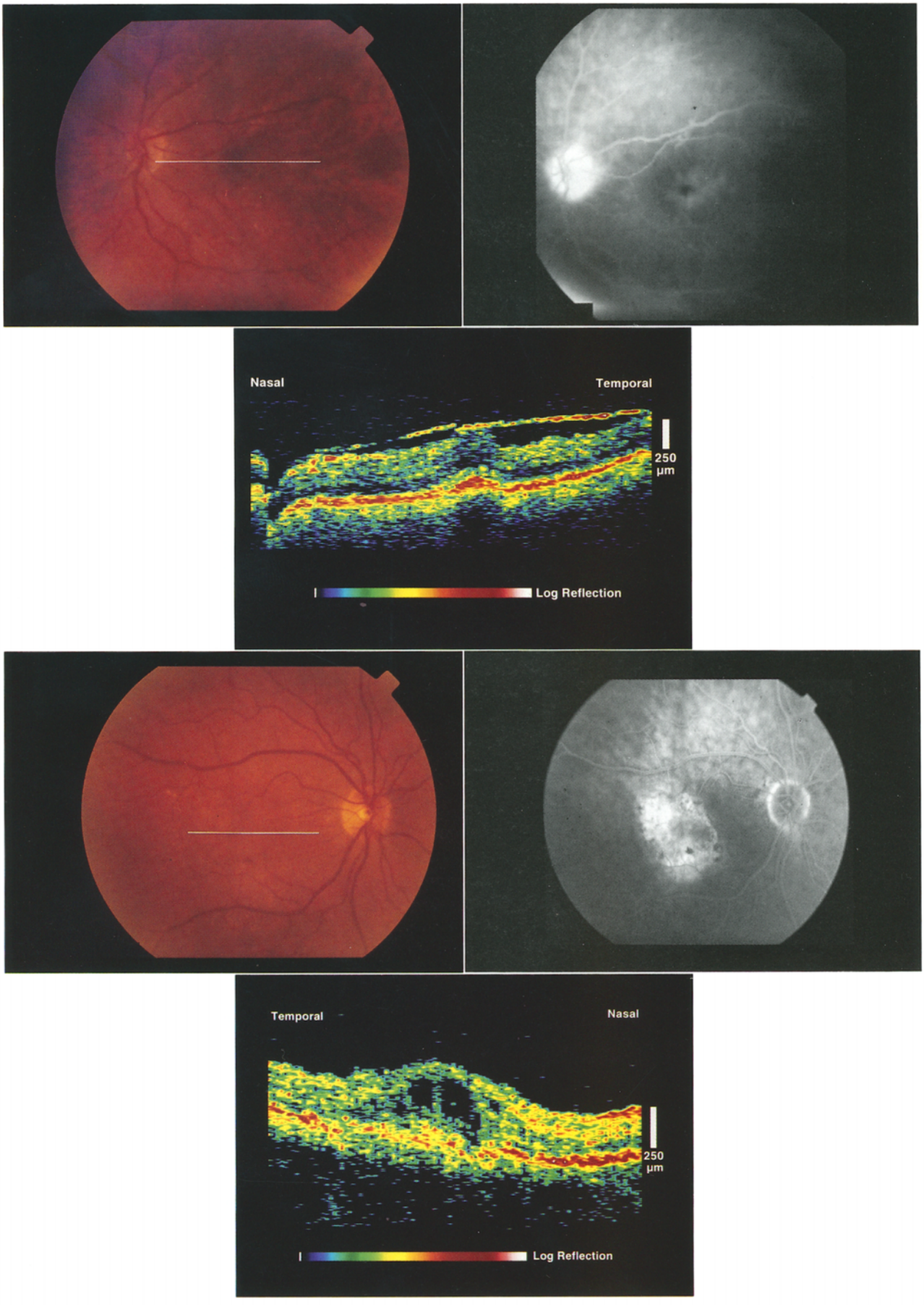
Nasal
Temporal
250 µm
Log Reflection
Temporal
Nasal
250 µm
Log Reflection

Top and **second row,** Figure 6. Case 4. Epiretinal membrane, left eye. **Top left,** fundus photograph. **Top right,** fluorescein angiogram with leakage consistent with cystoid macular edema. **Second row,** optical coherence tomography image depicts the epiretinal membrane, a foveal disruption attributed to macular edema, and vitreal displacement of the choroid and retina.

Third row and **bottom,** Figure 7. Case 5. Cystoid macular edema and hemorrhage, right eye. **Third row left,** fundus photograph. **Third row right,** fluorescein angiogram shows mottled hyperfluorescence in the central macula. **Bottom,** optical coherence tomography image reveals localized, nonreflective cystoid spaces, large central cysts, and a disruption in the retinal pigment epithelium and choriocapillaris.

quality of the eye and the pupil aperture. The minimum achievable transverse resolution is determined by the probe beam diameter at the retina, and was calculated to be 13 μm based on the Gullstrand schematic eye. We have discussed other determinants of transverse resolution elsewhere.[11]

The probe beam is delivered to the retina through a pair of orthogonal scanning mirrors to provide lateral beam positioning. The beam is coincident with the observation path of the slit lamp to allow simultaneous fundus examination and image acquisition. Computer control and data acquisition enable arbitrary scanning patterns on the fundus and provide a realtime display of the tomograph in progress on a monitor. Less than 200 μW of an 830-nm probe light is incident on the fundus, consistent with the ANSI recommended exposure limit for permanent intrabeam viewing.[13]

A +78-diopter condensing lens mounted in front of the eye provides an indirect image of the retina, which is used for both slit-lamp visualization of the fundus and OCT scanning. A single one-dimensional A-mode profile of optical reflectivity versus distance into the tissue is created by translating the reference arm mirror and measuring the magnitude of the interference signal at the detector. Two-dimensional, tomographic imaging of the retina is accomplished in manner analogous to ultrasound B-scan. In ultrasound B-mode, a cross-sectional image of acoustic reflectivity is created by obtaining multiple, single A-mode scans while rapidly scanning the probe beam through tissue. Similarly, a B-scan OCT image is constructed from a sequence of uniaxial A-mode longitudinal profiles of optical reflectivity, obtained while transversely scanning the probe beam across the retina. The OCT tomographs presented here are each composed of 100 A-mode scans and required a total of 2.5 seconds acquisition time. The images are displayed in false-color, where bright colors (red to white) correspond to regions of high relative optical reflectivity or backscattering, and dim colors (blue to black) represent areas of minimal or no relative reflectivity. A digital image processing algorithm is used to remove axial eye motion artifacts from the tomographs after data collection, and has been described elsewhere.[10] All the tomographs presented in this article are displayed two times expanded in the vertical direction for better image readability.

The location of the OCT probe beam on the fundus may be established either by slit-lamp observation of a visible light source placed coincident with the probe beam on the fundus, or by direct visualization of the probe beam and retina with an infrared sensitive video camera. For this study, the video camera was used, which has the advantage that a video frame grabber may be used to record the location and pattern of each OCT scan simultaneous with data acquisition. Also, near infrared rather than visible light may be used to illuminate the fundus, making the OCT examination well tolerated by patients. The +78-diopter condensing lens provides a field of view of approximately 35° through a dilated pupil, which was used for all patients in this study.

Optical coherence tomography was used to examine 51 eyes of 44 patients with macular diseases, including partial- and full-thickness macular hole, epiretinal membrane, macular edema, idiopathic central serous chorioretinopathy, detachment of the pigment epithelium, and choroidal neovascularization. Optical coherence tomographs were correlated with slit-lamp biomicroscopy, fundus photography, and fluorescein angiography.

An OCT image of the macular region (Fig 2) obtained from a healthy human subject establishes the correlation between known retinal anatomy and features evident on OCT tomographs. The inner margin of the retina is well defined due to the contrast between the nonreflective vitreous and the backscattering retina. The fovea is clearly identifiable from its characteristic morphology, including the foveal depression and the lateral displacement of the retina anterior to Henle's fiber layer. The posterior hyaloid barely appears as a membrane of low reflectance (blue) anterior to the foveal pit. The posterior aspect of the neurosensory retina is bounded in the OCT images by a highly reflective (red) band approximately 70 μm thick, which most likely corresponds to the choriocapillaris and retinal pigment epithelium (RPE). The region just anterior to the choriocapillaris typically shows weak backscattering in the OCT tomographs and corresponds in location and thickness to the photoreceptors. The inner and outer plexiform layers may be identifiable by their location and the increased backscatter signal compared to their nuclear layers. Another highly scattering (red) layer at the inner margin of the retina appears to have characteristics consistent with the nerve fiber layer.[11]

Results

Fifty-one eyes of 44 patients were examined with OCT for macular disease with the following clinical diagnoses: macular hole (9 eyes); epiretinal membrane (3 eyes); macular edema (8 eyes); idiopathic central serous chorioretinopathy, detachment of the RPE, and choroidal neovascularization (21 eyes); disciform scar (2 eyes); macular

dystrophy and drusen (4 eyes); chorioretinitis (2 eyes); laser injury (1 eye); and foreign body injury (1 eye). Results from selected cases are presented below. For each case,OCT sections are displayed along with accompanying fundus photographs which are marked to indicate the orientation of each of the OCT scans on the retina.

Selected Case Reports

Macular Hole

Case 1. A 55-year-old woman whose visual acuity was counting fingers at 7 feet in the right eye had a full-thickness idiopathic macular hole with a surrounding cuff of subretinal fluid (Fig 3, second row left). The OCT image shows several features characteristic of a stage 3 hole, including a sharply defined, full-thickness defect in the retina and a marginal halo of retinal detachment (Fig 3, second row right). The presence of small, nonreflective spaces in the outer plexiform and inner nuclear layers is observed, consistent with cystoid changes.

Case 2. A 72-year-old woman had a full-thickness macular hole and operculum (Fig 4, third row left) with visual acuity of 20/300 in the left eye. The OCT image shows a complete defect within the neurosensory retina (Fig 4, third row right). A highly reflective tag contiguous with the internal limiting membrane is observed, consistent with retinal tissue and the biomicroscopic observation of the operculum.

Case 3. A 73-year-old woman with a lamellar macular hole and visual acuity of 20/20 in the left eye was studied (Fig 5, bottom left). The OCT tomograph displays a partial depletion of retinal tissue (Fig 5, bottom right). A moderately reflective layer of residual tissue appears to span the entire hole, confirming the clinical diagnosis of a partial-thickness hole.

Epiretinal Membrane

Case 4. An 84-year-old man had a visual acuity of 20/200 in the left eye with the clinical diagnosis of an epiretinal membrane in the macular area (Fig 6, top left). The retinal arterioles superior to the fovea appeared to be straightened. Fluorescein angiography showed late leakage of fluorescein in a petalloid pattern consistent with cystoid macular edema (Fig 6, top right). The OCT scan shows the presence of a highly reflective membrane on the surface of the retina (Fig 6, second row). The neurosensory layer of the fovea appears to be disrupted, and small areas of minimal backscattering are observed within the neurosensory retina that may be attributed to macular edema. A vitreal displacement of the choroid and retina is also apparent, which may be related to the presence of macular edema or traction of the epiretinal membrane on the retina.

Macular Edema

Case 5. An 80-year-old woman with age-related macular degeneration had cystoid macular edema and a small amount of hemorrhage associated with a poorly defined choroidal neovascular membrane in the right eye (Fig 7, third row left). Visual acuity was counting fingers at 3 feet. Mottled hyperfluorescence in the central macula was seen in late views of the fluorescein angiogram, consistent with macular edema (Fig 7, third row right). An OCT image obtained from this patient shows highly localized, nonreflective cystoid spaces in the outer plexiform and inner nuclear layers and large central cysts that extended almost to the internal limiting membrane (Fig 7, bottom). The reflective band corresponding to the RPE and choriocapillaris also appears to be disrupted in the image. Retinal thickness, measured directly from the OCT tomogram, varies from 270 μm temporally to approximately 360 μm in the cystic areas.

Case 6. A 20-year-old woman had a central retinal vein occlusion and macular edema in the left eye (Fig 8, top left). Visual acuity was 20/400. Fluorescein angiography showed late leakage of fluorescein throughout the posterior pole (Fig 8, top right). On OCT, disruption of the layers of the retina with localized areas of low reflectance, consistent with fluid accumulation in the outer retinal layer, was demonstrated (Fig 8, second row). The outer plexiform layer appears to be specifically involved, consistent with the classically described histopathologic findings of macular edema. Retinal thickness as determined from the image increases from 250 μm nasally to 690 μm at its thickest point in the tomogram.

Diabetic Retinopathy

Case 7. An 87-year-old woman with diabetes mellitus and hypertension was evaluated for background diabetic retinopathy and clinically significant macular edema (Fig 9, third row left). Slit-lamp biomicroscopy of the right eye showed retinal thickening along the superotemporal arcade with hard exudate extending into the macula. Visual acuity was 20/40. A horizontal OCT section acquired just superior to the fovea in this eye depicts increased retinal thickness nasally, with the development of an optically clear space in the outer retina, consistent with cystic changes (Fig 9, third row right). Focal areas of high backscattering are noted in the center of the image and correspond to foveal exudate. Retinal thickness, measured from the tomogram, varies from 200 μm temporally to 620 μm at the point of maximum thickness in the image.

Case 8. A 66-year-old woman with background diabetic retinopathy and macular edema in the left eye was examined

Top and second row, Figure 8. Case 6. Central retinal vein occlusion and macular edema, left eye. **Top left,** fundus photograph. **Top right,** fluorescein angiogram shows diffuse late leakage. **Second row,** optical coherence tomography image shows disruption of the retinal layers and areas of low reflectivity consistent with fluid accumulation.

Third row, Figure 9. Case 7. Background diabetic retinopathy and macular edema, right eye. **Third row left,** fundus photograph. **Third row right,** optical coherence tomography section demonstrates fluid accumulation and retinal thickening temporally, and focal areas of high reflectance corresponding to retinal exudate.

Bottom, Figure 10. Case 8. Background diabetic retinopathy, macular edema, and foveal hard exudate, left eye. **Bottom left,** fundus photograph. **Bottom right,** optical coherence tomography image depicts a focal area of high backscattering corresponding to the exudate and increased retinal thickness consistent with macular edema. The high reflectivity of the exudate shadows the backscattering from the choroid and pigment epithelium below.

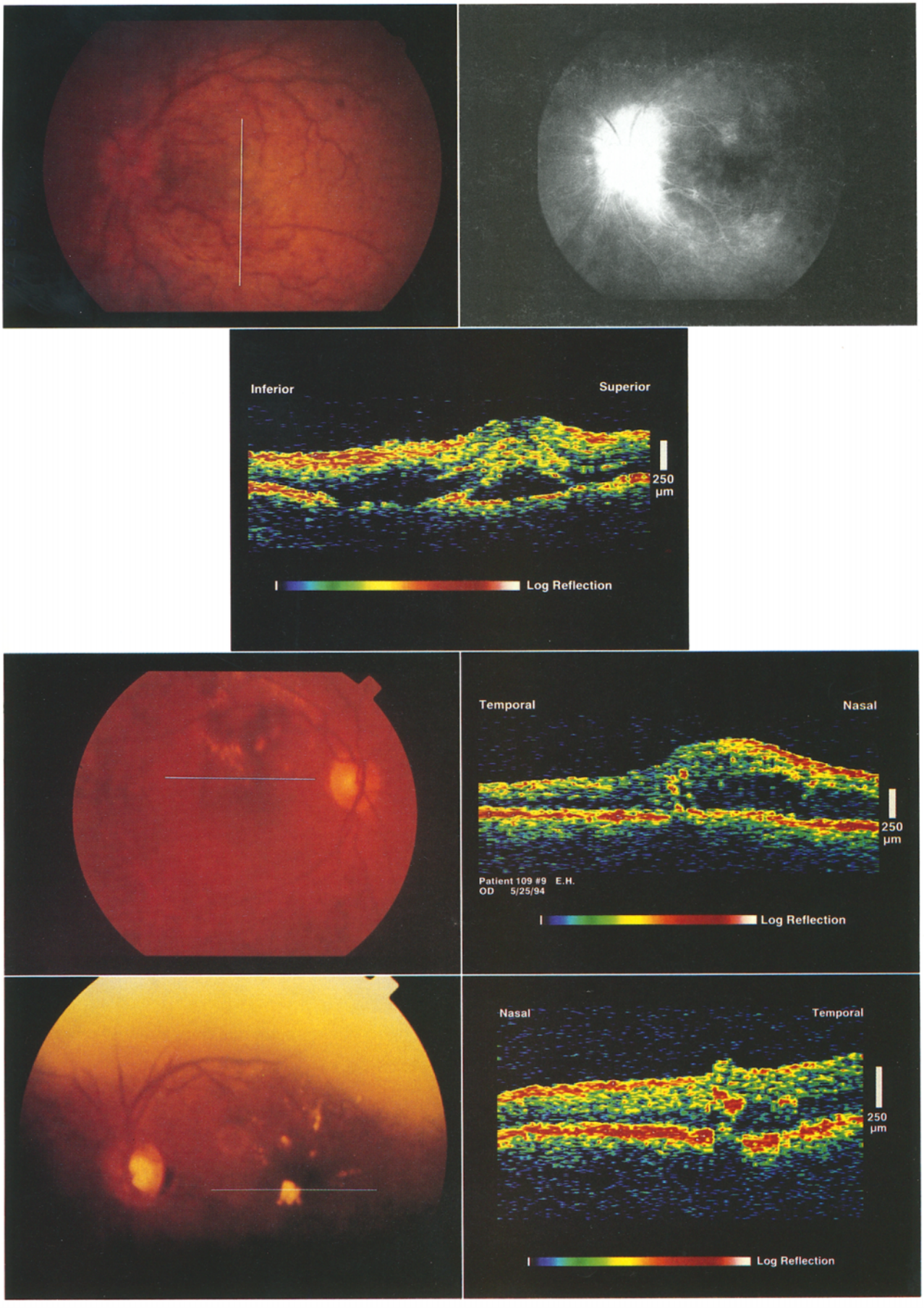
Inferior
Superior
250
µm
Log Reflection
Temporal
Nasal
250
µm
Patient 109 #9 E.H.
OD 5/25/94
Log Reflection
Nasal
Temporal
250
µm
Log Reflection

(Fig 10, bottom left). Visual acuity in this eye was 20/40. Foveal hard exudate and retinal thickening were observed on slit-lamp biomicroscopy. The OCT image demonstrates focal areas of high reflectance (red) within the neurosensory retina, corresponding to the foveal hard exudate which shadows deeper structures (Fig 10, bottom right). Disruption of the neurosensory retina also is evident, and a space of low reflectance between the neurosensory retina and the RPE is consistent with the clinical observation of retinal thickening. Retinal thickness, as determined from the OCT image, increases from 220 μm nasally to 360 μm temporally.

Detachments of the Retinal Pigment Epithelium and Neurosensory Retina

Case 9. A 34-year-old man was evaluated 3 weeks after the onset of idiopathic central serous chorioretinopathy in the left eye (Fig 11, top left). His visual acuity was 20/40. Fluorescein angiography showed a focal region of hyperfluorescence nasal to the fovea (Fig 11, top right). An OCT image obtained through the optic disc and serous detachment shows the contour of the disc and separation of the neurosensory retina from the highly reflective (red) band corresponding to the RPE and choriocapillaris (Fig 11, second row left; Fig 11, second row right, black line). An OCT section taken directly through the fovea also demonstrates an elevation of the retina with the development of an optically clear space consistent with subretinal fluid accumulation and detachment of the neurosensory retina (Fig 11, second row right; Fig 11, top left, white line). The brightly backscattering RPE appears intact below the fluid-filled space, except in the region directly beneath the fovea. An area of increased reflectivity (red) is observed in the fovea, which may be due to normal incidence of the probe beam, and results in shadowing of the RPE and choriocapillaris below. The height of retinal elevation directly beneath fovea was measured from the image to be 260 μm. The patient received focal photocoagulation treatment with a yellow dye laser and returned 1 month later for examination (Fig 11, third row left). Visual acuity had improved to 20/20, and no subretinal fluid was noted on slit-lamp biomicroscopy. An OCT image taken through the foveal region demonstrates no retinal detachment and is consistent with the clinical observation of resolution (Fig 11, third row right).

Case 10. A 57-year-old-man was examined 1 day after the onset of central visual loss in the left eye, with a visual acuity of 20/25. He received a diagnosis of neurosensory detachment of the retina associated with idiopathic central serous chorioretinopathy (Fig 12, bottom left). Horizontal OCT sections were acquired through the neurosensory detachment (Fig 12, bottom right). In each of the sections, an elevation of the retina above an optically clear, fluid-filled space is noted, consistent with a detachment of the neurosensory retina. An intact, brightly backscattering layer below the subretinal fluid retains the contour of the globe and corresponds to the RPE and choriocapillaris. The height of the detachment was measured directly under the fovea in OCT section (Fig 12, bottom right) and was 240 μm.

Case 11. A 41-year-old man had both a neurosensory detachment and an RPE detachment of the macula in the right eye, which were associated with the diagnosis of idiopathic central serous chorioretinopathy (Fig 13, top left). His visual acuity was 20/40. Fluorescein angiography displayed filling of a small RPE detachment temporal to the fovea and hyperfluorescence along the superotemporal arcade in the temporal macula, consistent with a neurosensory detachment of the retina (Fig 13, top right). Through both areas of retinal pathology, OCT images were obtained. A tomograph taken through the area of RPE detachment toward the optic disc shows elevation of both the retina and a thin, brightly backscattering layer corresponding to the RPE (Fig 13, second row left). The optically clear space seen below the neurosensory retina and the RPE is consistent with the serous fluid and the diagnosis of RPE detachment. The choroidal tissue beneath the detachment is shadowed by the highly backscattering RPE above, which may be more reflective when detached due to the interface with the serous fluid. The adjacent normal retina in the image shows that the reflective band corresponding to the RPE and choriocapillaris is thicker than the detached RPE alone. The maximum retinal elevation was 290 μm from the OCT section. An OCT image taken through the area of the neurosensory detachment shows elevation of the neurosensory retina and a large area of low reflectivity, consistent with a fluid-filled space (Fig 13, second row right). The reflective band corresponding to RPE and choriocapillaris in this image appears intact beneath the serous fluid cavity, except where it is shadowed by retinal blood vessels. The height of the fluid-filled cavity reaches a maximum of 590 μm in the OCT image.

Four months later, the patient had spontaneous resolution of the neurosensory detachment, but persistence of the RPE detachment in the right eye (Fig 13, third row left). Fluorescein angiography again showed filling of a small RPE detachment temporal to the fovea, but there was no evidence of the previous neurosensory detachment in the superior macula (Fig 13, third row right). An OCT image taken through the RPE detachment and the fovea demonstrates continued elevation of both the retina and the thin, reflective layer corresponding to the RPE (Fig 13, bottom left) above an optically clear, fluid-filled cavity. Backscattering from the surface of the choriocapillaris is barely visible below the serous cavity due to attenuation of light from the highly reflective detached RPE. The configuration of the serous cavity appears to have minimally changed from the previous examination, with a measured detachment of 240 μm. In con-

Top, second, and **third rows,** Figure 11. Case 9. Idiopathic central serous chorioretinopathy, left eye. **Top left,** fundus photograph shows a neurosensory detachment directly in the fovea. **Top right,** fluorescein angiogram demonstrates a focal area of hyperfluorescence, consistent with central serous chorioretinopathy. **Second row left,** optical coherence tomography (OCT) section obtained through the optic disc and neurosensory detachment displays elevation of the neurosensory retina above a nonreflective fluid-filled space, and a reflective (red) band corresponding to the retinal pigment epithelium and choriocapillaris (black line shown on fundus). The optic disc cup also is well delineated. **Second row right,** OCT image taken directly through the fovea also demonstrates detachment of the neurosensory retina (white line shown on fundus). **Third row left,** fundus photograph taken 1 month after laser photocoagulation treatment. **Third row right,** OCT section obtained through the fovea shows resolution of the neurosensory detachment.

Bottom, Figure 12. Case 10. Idiopathic central serous chorioretinopathy, left eye. **Bottom left,** fundus photograph depicts a neurosensory detachment (arrows). **Bottom right,** serial horizontal optical coherence tomography sections demonstrate elevation of the neurosensory retina; an optically clear, fluid-filled cavity; and backscattering from the intact retinal pigment epithelium and choriocapillaris below the fluid accumulation.

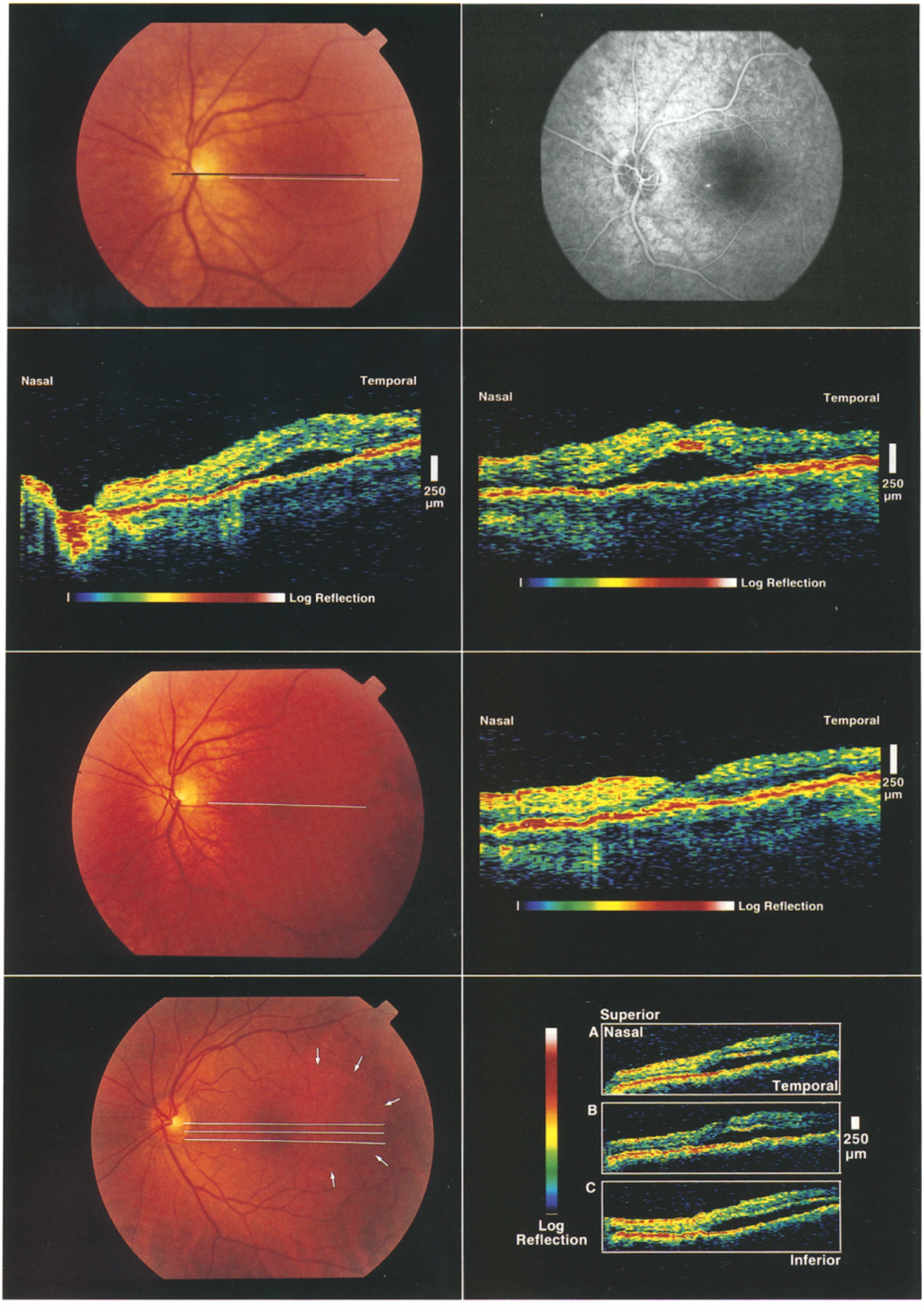
Nasal
Temporal
250 µm
Log Reflection
Nasal
Temporal
250 µm
Log Reflection
Nasal
Temporal
250 µm
Log Reflection
Superior
A
Nasal
Temporal
B
C
250 µm
Log Reflection
Inferior

trast, a tomograph taken through the area of previous neurosensory detachment shows no evidence of retinal elevation or subretinal fluid accumulation, consistent with the clinical observation of resolution (Fig 13, bottom right).

Case 12. A 41-year-old woman had laser photocoagulation in the right eye for treatment of an idiopathic choroidal neovascular membrane (Fig 14, top left). Her visual acuity was 20/60. A recurrent choroidal neovascular membrane was observed that was associated with retinal hemorrhage and neurosensory detachment of the retina. Fluorescein angiography showed late staining of the scar and moderate leakage of fluorescein (Fig 14, top right). Optical coherence tomography scanning demonstrates disruption of the layers of the neurosensory retina in the area that corresponds to the laser scar and a contiguous area of low reflectance consistent with the serous fluid accumulation and neurosensory detachment of the retina (Fig 14, bottom left; Fig 14, top left, white line). The reflective band corresponding to the RPE and choriocapillaris remains intact under the fluid-filled cavity. The neurosensory detachment reaches a maximum height of 250 μm in the image. Serial vertical sections through the macula (Fig 14, bottom right; Fig 14, top left, black lines) provide three-dimensional information on the extent of the detachment and show temporal retina (1), the neurosensory detachment (2–4), and evidence of disruption of the retinal layers corresponding to the fibrovascular scar (4–6).

Discussion

Optical coherence tomography is a new imaging modality that can provide high-resolution cross-sectional tomographs of retinal pathology in vivo. Because OCT imaging is noninvasive and uses infrared illumination of the fundus, the technique appears to be more comfortable and better tolerated by patients than either fluorescein angiography or fundus photography. The 10-μm axial resolution of OCT is better than other noninvasive imaging techniques in the posterior segment of the eye, including standard[1] and high-frequency ultrasound,[2,3] scanning laser tomography,[4] scanning laser ophthalmoscopy,[5] and other methods of measuring retinal or nerve fiber layer thickness.[14,15] High longitudinal resolution may be important for the clinical evaluation of many macular diseases, including macular holes, macular edema, retinal detachment, and choroidal neovascularization.

Cross-sectional imaging of the fovea with OCT is potentially useful in diagnosing and monitoring macular hole progression. Optical coherence tomography images obtained from patients with full-thickness macular holes show several characteristic histologic features, including a sharply defined, full-thickness excavation of the retina, a marginal halo of retinal detachment, and the presence of small, nonreflective cysts in the outer plexiform and inner nuclear layers. While the pathogenesis of idiopathic macular hole formation is incompletely understood, several studies have implicated the importance of vitreoretinal traction in hole development.[16] Pars plana vitrectomy may halt the development of full-thickness holes in high-risk patients.[17] Cross-sectional imaging with OCT may be useful in identifying and monitoring these high-risk eyes, particularly in the fellow eyes of patients with macular holes. Distinction between a full-thickness macular hole and a lamellar hole is also possible from the cross-sectional view, as is identification of an associated operculum. Separation of the posterior hyaloid membrane in the foveal region may reduce the risk of hole formation.[18] Optical coherence tomography may be able to assess the vitreoretinal interface with higher resolution than kinetic ultrasound, which can only detect a minimum separation of 500 μm.[18] Distinction between epiretinal membrane and retinal tissue, both displaying high reflectance, from the posterior hyaloid which is minimally reflective is also possible.

Optical coherence tomography may be useful in measuring changes in retinal thickness, which accompanies many retinal diseases and diseases of the optic nerve. Abnormal fluid accumulation in the retina results in the clinical and angiographic findings of increased thickness of the neurosensory retina and macular edema, respectively. Fluorescein angiography is used routinely to determine the presence of macular edema. While angiography may determine the presence and the source of the edema fluid, it is not always a reliable indicator of areas of retinal or RPE dysfunction. Measurements of increased retinal thickness have been found to correlate more strongly with reduced visual acuity than observations of fluorescein leakage.[19] Optical coherence tomography quantitatively can assess retinal thickness and edema with a 10-μm longitudinal resolution, exceeding the comparatively limited sensitivity of slit-lamp biomicroscopy and stereo fundus photography to changes in retinal thickness.[20]

Linear OCT sections of the macula provide a means of identifying, localizing, and quantifying edematous changes. Tomographs obtained from patients with macular edema secondary to venous occlusion show local areas of retinal thickening, measured from the vitreo-

Figure 13. Case 11. Idiopathic central serous chorioretinopathy and detachment of the retinal pigment epithelium (RPE), right eye. **Top left,** fundus photograph shows a neurosensory detachment along the superotemporal arcade (arrows) and an RPE detachment temporal to the fovea (arrowhead). **Top right,** fluorescein angiogram shows a detachment of the pigment epithelium temporal to the fovea and a neurosensory retinal detachment in the superior macula. **Second row left,** optical coherence tomography (OCT) taken through the RPE detachment shows retinal and RPE elevation; a thin, bright scattering layer corresponding to the detached RPE; and an intact adjacent RPE and choriocapillaris. **Second row right,** OCT image obtained through the neurosensory retinal detachment shows retinal elevation and a fluid-filled space above a normal RPE and choriocapillaris. **Third row left,** fundus photograph obtained 4 months after spontaneous resolution of the neurosensory detachment. **Third row right,** fluorescein angiogram after 4 months shows the RPE detachment and no evidence of the neurosensory detachment. **Bottom left,** OCT image through the RPE detachment shows elevation of the retina and RPE above a serous cavity. **Bottom right,** OCT image confirms spontaneous resolution of the neurosensory detachment after 4 months.

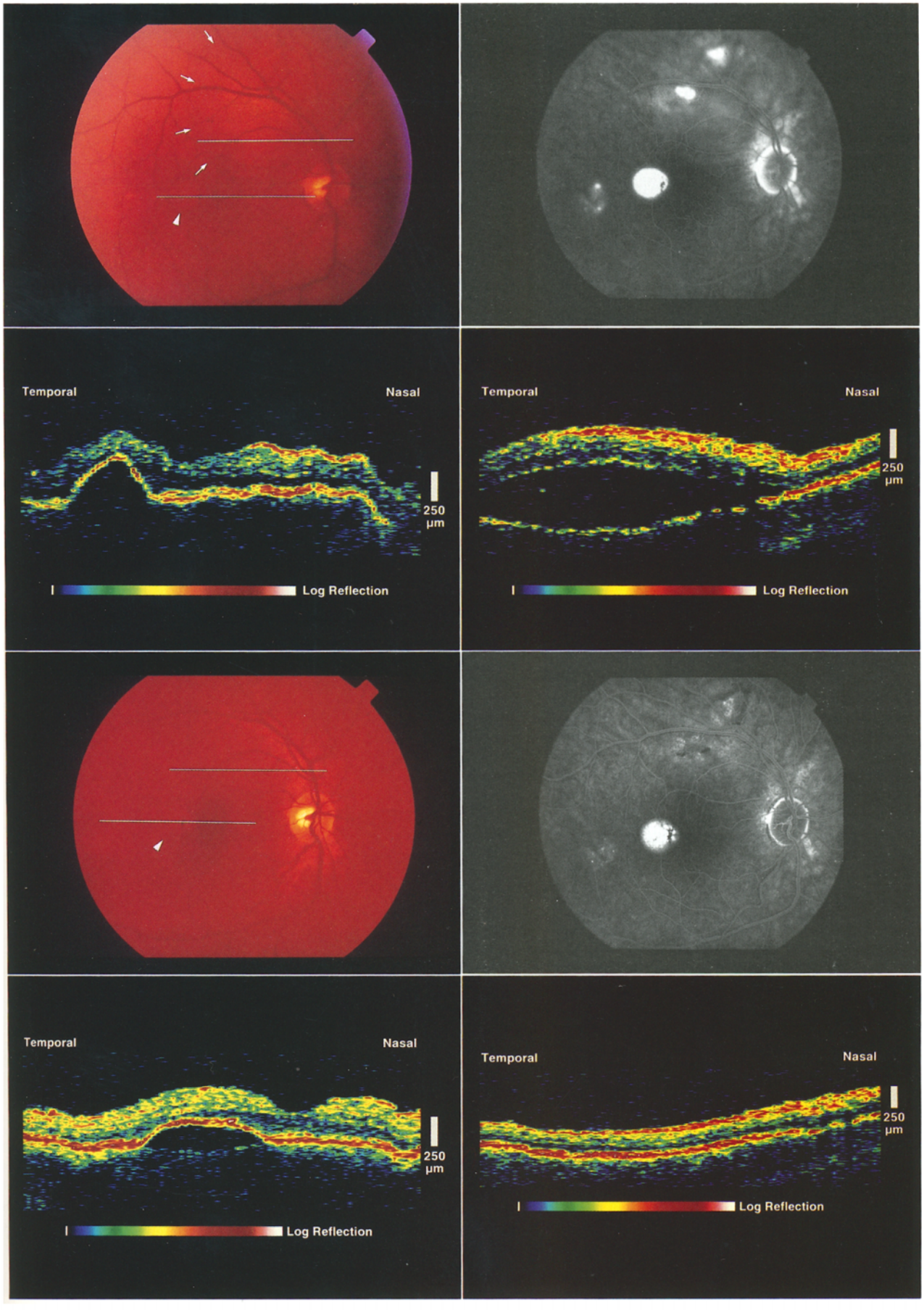
Temporal
Nasal
250 µm
Log Reflection
Temporal
Nasal
250 µm
Log Reflection
Temporal
Nasal
250 µm
Log Reflection
Temporal
Nasal
250 µm
Log Reflection

retinal interface to the highly scattering (red) outer layer corresponding to the choriocapillaris and pigment epithelium. Optical coherence tomography images obtained from patients with cystoid macular edema closely correspond to the known histopathology demonstrating the highly localized, nonreflective cystoid spaces in the outer plexiform and inner nuclear layers, and large central cysts which extend almost to the internal limiting membrane. Focal areas of high reflectance were identified within the neurosensory retina corresponding to exudate observed within the macula and in contrast to the very low reflectance observed with intraretinal or subretinal fluid associated with retinal detachment. In patients with age-related macular degeneration and choroidal neovascularization, intraretinal spaces of relatively low backscattering were observed, and the band corresponding to the RPE and choriocapillaris appeared to be thickened and disrupted. In contrast, the RPE and choriocapillaris appeared to be normal in cases where macular edema was due to a retinal vascular etiology. These images indicate that OCT may be useful as an adjunct or as a noninvasive alternative to angiography for diagnosing or confirming macular edema and exudate. Optical coherence tomography images, in analogy to ultrasound M-scan (multiple A-scans of single selected points) on the macula identified through linear OCT section, also could allow one to track interval changes in retinal thickness at desired locations with better than 10-μm axial resolution, because successive scans comprising the M-scan could be averaged. These point measurements would enable highly accurate monitoring of fluid accumulation, or the resolution of edema after photocoagulation therapy.

Detachment of the neurosensory retina and the RPE also was studied. Optical coherence tomography images of serous RPE and pigment epithelial detachment demonstrate the accumulation of optically clear fluid in the subretinal and the sub-RPE spaces. Tomographs of serous neurosensory detachments show an elevation of the neurosensory retina, a nonreflective fluid-filled subretinal space, and a highly reflective band corresponding to the RPE and choriocapillaris that appears to retain the contour of the globe. In comparison, eyes with RPE detach-

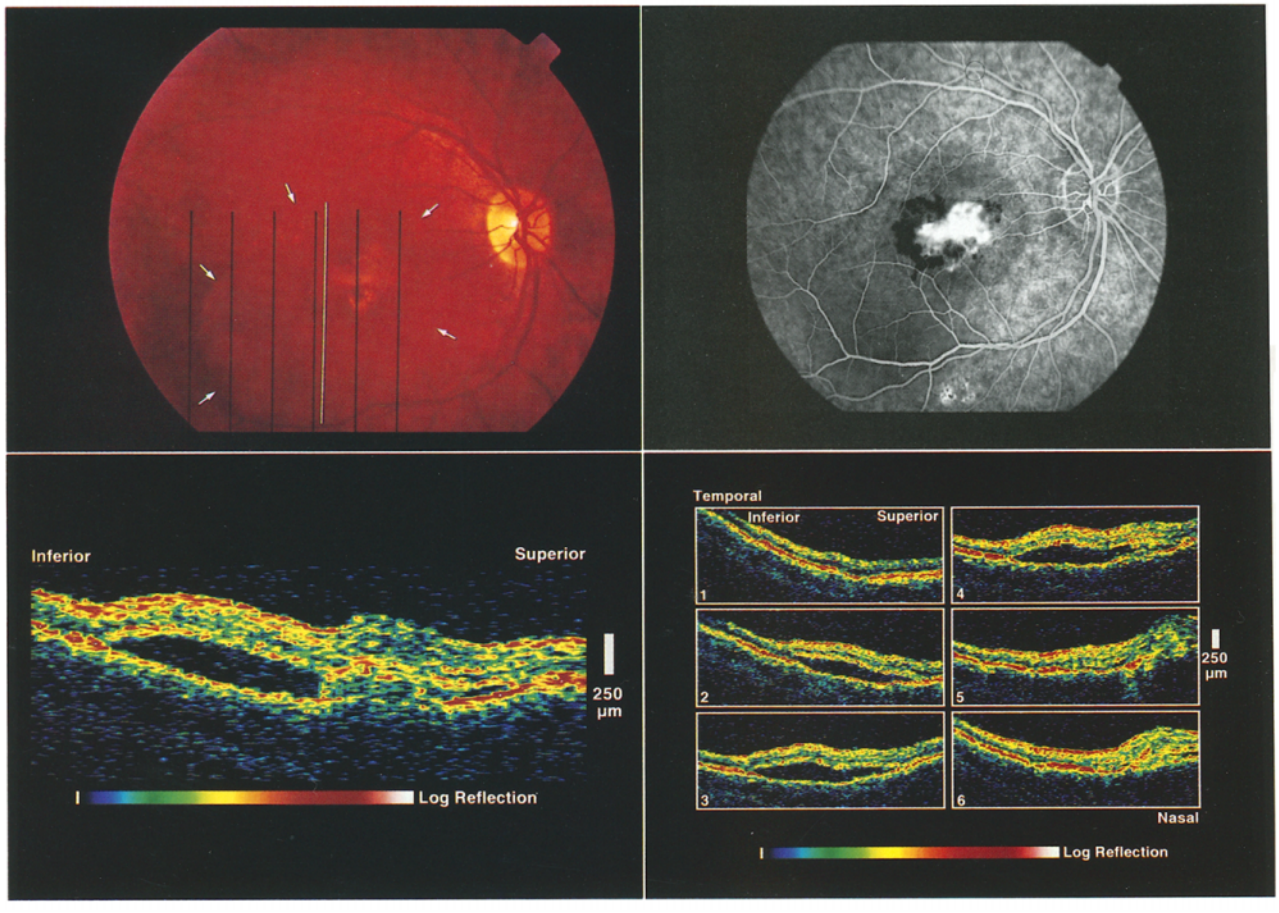

Figure 14. Case 12. Idiopathic choroidal neovascularization and neurosensory retinal detachment after laser photocoagulation treatment, right eye. **Top left,** fundus photograph with the neurosensory detachment outlined (arrows). **Top right,** fluorescein angiogram shows moderate leakage corresponding to a neurosensory retinal detachment and late staining of the laser scar. **Bottom left,** optical coherence tomography image shows elevation of the neurosensory retina and disruption of the retina corresponding to the retinal detachment and laser scar respectively (white line on fundus photograph). **Bottom right,** serial vertical sections taken through the macula provide three-dimensional information on the extent of the detachment and laser scar (black lines on fundus photograph).

ments display a thin, highly backscattering layer just beneath the neurosensory retina corresponding to the RPE. This layer appears separated from the contour of the globe and above the fluid-filled space as expected. In these eyes, the reflective layer corresponding to the detached RPE is thinner than the band corresponding to the normal surrounding RPE and choriocapillaris, confirming that the RPE and choriocapillaris normally appear together as highly backscattering in the OCT images. High backscattering from the detached RPE appears to shadow deeper structures, such as the choriocapillaris, and may result from the refractive index boundary between the RPE and serous fluid, or morphologic changes in the RPE cells themselves. These results show that OCT is capable of distinguishing detachments of the neurosensory retina from detachments of the RPE.

Optical coherence tomography images of detachments of the pigment epithelium point out that deep structures in the retina may be affected by light penetration through intervening retinal layers. Similarly, it was noted that high backscattering from intraretinal hard exudate shadows the reflections from the choriocapillaris and pigment epithelium below. The OCT instrument is sensitive primarily to unscattered probe light,[11] which exponentially attenuates as it propagates through the retina. The tomograms are displayed on a logarithmic reflectivity scale to partially compensate for this attenuation; however, it is still important to note that a highly absorbing or reflecting layer in the retina, such as hard exudate or a retinal blood vessel,[11] will cause the backscatter signal from deeper retinal structures to appear unusually dim.

We previously have shown that OCT is potentially useful for profiling the contour of the optic nerve head, including cupping, and for measuring retinal and nerve fiber layer thickness. Quantitation of nerve fiber layer thickness in the peripapillary region is directly relevant to the early diagnosis and monitoring of glaucoma, where intraocular pressure often does not reliably affect disease progression,[21] ophthalmoscopy and stereo fundus photography are subjective,[22] and visual field defects occur only after irreversible damage to the nerve fiber layer.[23]

In conclusion, OCT is a new technique for the clinical evaluation of a variety of macular diseases. These preliminary images suggest that OCT may be particularly useful in the more sensitive diagnosis and quantitative monitoring of macular holes, macular edema, and retinal detachment. Variations in OCT backscattering signal also may provide a means of identifying other retinal and choroidal pathologies, including choroidal nevi, hemorrhagic exudate, tumors, and other inflammatory diseases. Further research is needed to determine whether OCT imaging may be applicable to the localization of choroidal neovascular membranes and the evaluation of other inflammatory and degenerative diseases of the retina.

References

1. Olsen T. The accuracy of ultrasonic determination of axial length in pseudophakic eyes. Acta Ophthalmol 1989;67: 141–4.
2. Pavlin CJ, Sherar MD, Foster FS. Subsurface ultrasound microscopic imaging of the intact eye. Ophthalmology 1990;97:244–50.
3. Pavlin CJ, Harasiewicz K, Sherar MD, Foster FS. Clinical use of ultrasound biomicroscopy. Ophthalmology 1991;98: 287–95.
4. Webb RH, Hughes GW, Delori FC. Confocal scanning laser ophthalmoscope. Appl Opt 1987;26:1492–9.
5. Bille JF, Dreher AW, Zinser G. Scanning laser tomography of the living human eye. In: Masters BR, ed. Noninvasive Diagnostic Techniques in Ophthalmology. New York: Springer-Verlag, 1990; chap. 28.
6. Huang D, Wang J, Lin CP, et al. Micron-resolution ranging of cornea and anterior chamber by optical reflectometry. Lasers Surg Med 1991;11:419–25.
7. Swanson EA, Huang D, Hee MR, et al. High-speed optical coherence domain reflectometry. Opt Lett 1992;17:151–3.
8. Hee MR, Huang D, Swanson EA, Fujimoto JG. Polarization-sensitive low-coherence reflectometer for birefringence characterization and ranging. J Opt Soc Am [B] 1992;9: 903–8.
9. Huang D, Swanson EA, Lin CP, et al. Optical coherence tomography. Science 1991;254:1178–81.
10. Swanson EA, Izatt JA, Hee MR, et al. In vivo retinal imaging by optical coherence tomography. Opt Lett 1993;18:1864–6.
11. Hee MR, Izatt JA, Swanson EA, et al. Optical coherence tomography of the human retina. Arch Ophthalmol (in press).
12. Izatt JA, Hee MR, Swanson EA, Huang D, Lin CP, Schuman JS, Puliafito CA, Fujimoto JG. Optical coherence tomography of the human anterior segment. Arch Ophthalmol (in press).
13. The Laser Institute of America. American National Standard for the Safe Use of Lasers. Toledo, OH: The Institute, 1986;34. (ANSI Z136.1.1986).
14. Shahidi M, Zeimer RC, Mori M. Topography of the retinal thickness in normal subjects. Ophthalmology 1990;97:1120–4.
15. Weinreb RN, Dreher AW, Coleman A, et al. Histopathologic validation of fourier-ellipsometry measurements of retinal nerve fiber layer thickness. Arch Ophthalmol 1990;108:557–60.
16. Gass JDM. Idiopathic senile macular hole. Its early stages and pathogenesis. Arch Ophthalmol 1988;106:629–39.
17. de Bustros S. Early stages of macular holes. To treat or not to treat [editorial]. Arch Ophthalmol 1990;108:1085–6.
18. Fisher YL, Slakter JS, Yannuzzi LA, Guyer DR. A prospective natural history study and kinetic ultrasound evaluation of idiopathic macular holes. Ophthalmology 1994;101:5–11.
19. Shahidi M, Ogura Y, Blair NP, et al. Retinal thickness analysis for quantitative assessment of diabetic macular edema. Arch Ophthalmol 1991;109:1115–19.
20. Nussenblatt RB, Kaufman SC, Palestine AG, et al. Macular thickening and visual acuity. Measurement in patients with cystoid macular edema. Ophthalmology 1987;94:1134–9.
21. Sommer A. Intraocular pressure and glaucoma. Am J Ophthalmol 1989;180:485.
22. Tielsch JM, Katz J, Quigley HA, et al. Intraobserver and interobserver agreement in measurement of optic disc characteristics. Ophthalmology 1988;95:350–6.
23. Quigley HA, Addicks EM, Green WR. Optic nerve damage in human glaucoma. III Quantitative correlation of nerve fiber loss and visual field defect in glaucoma, ischemic neuropathy, papilledema, and toxic neuropathy. Arch Ophthalmol 1982;100:146.